

Quantum measurement with recycled photons

Eyal Buks  and Banoj Kumar Nayak *Andrew and Erna Viterbi Department of Electrical Engineering, Technion, Haifa 32000, Israel*

(Received 16 October 2021; revised 12 December 2021; accepted 10 January 2022; published 18 January 2022)

We study a device composed of an optical interferometer integrated with a ferrimagnetic sphere resonator (FSR). Magneto-optic coupling can be employed in such a device to manipulate entanglement between optical pulses that are injected into the interferometer and the FSR. The device is designed to allow measuring the lifetime of such macroscopic entangled states in the region where environmental decoherence is negligibly small. This is achieved by recycling the photons interacting with the FSR in order to eliminate the entanglement before a pulse exits the interferometer. The proposed experiment may provide some insight into the quantum to classical transition associated with a measurement process.

DOI: [10.1103/PhysRevB.105.014421](https://doi.org/10.1103/PhysRevB.105.014421)

I. INTRODUCTION

Consider two successive quantum measurements [1]. In the first one, which is performed at time t_1 , the observable A_1 is being measured, whereas in the second one, which is performed at a later time $t_2 \geq t_1$, the observable A_2 is being measured. Let \mathcal{A}_1 (\mathcal{A}_2) be the outcome of the first (second) measurement and $\{a_{n,k}\}_k$ be the set of eigenvalues of the observable A_n , where $n \in \{1, 2\}$. The probability that the measurement at time t_2 of the observable A_2 yields the value a_{2,k_2} , namely, the probability that $\mathcal{A}_2 = a_{2,k_2}$, is denoted by $p_2(k_2)$. Two methods for the calculation of $p_2(k_2)$ are considered below. In the first one, the time evolution from an initial time $t_0 < t_1$ to time t_2 is assumed to be purely unitary, and the probability $p_2(k_2)$ for the measurement at time t_2 is calculated using the Born rule. The second method is based on the assumption that the unitary evolution is disturbed at time t_1 , at which the density operator of the system undergoes a collapse [2–8] corresponding to the measurement of the observable A_1 . Note that for both methods the coupling between the quantum subsystem and its measuring apparatus is taken into account in the unitary time evolution [9–13]. Under what conditions is the probability $p_2(k_2)$ affected [14] by whether a collapse has occurred or has not occurred at the earlier time t_1 ?

A sufficient condition, which ensures that the collapse at time t_1 has no effect on the probability $p_2(k_2)$, is discussed below. This sufficient condition can be expressed as $[A_2(t_2), A_1(t_1)] = 0$, where $A_1(t_1)$ and $A_2(t_2)$ are the Heisenberg representations of the A_1 and A_2 operators, respectively [see Eq. (A11) in Appendix A]. As is explained below, this condition is satisfied for the vast majority of experimental setups used to study quantum systems.

Commonly, the entire system can be composed of a quantum subsystem (QS) under study and one or more ancilla subsystems (ASs) that are used for probing the QS. Moreover, very commonly, the process of measurement is based on the scattering of AS particles (electrons, photons, phonons, magnons, etc.) by the QS under study. In such a scattering process, the QS is bombarded by incoming AS particles. The

properties of the QS are inferred from measured properties of the scattered AS particles. For this type of measurement the observables A_1 and A_2 are operators of the AS and are independent of the degrees of freedom of the QS.

For the above-discussed two successive measurements of a given QS, two cases are considered below. For the first one, which is the common case, the ancilla particles that are used for the first measurement are not used for the second one. The two independent ASs associated with the two successive measurements are denoted by AS1 and AS2. For this case the observable A_1 (A_2) is an operator of AS1 (AS2), and consequently, the condition $[A_2(t_2), A_1(t_1)] = 0$ is satisfied; therefore, any collapse-induced effect on the probability $p_2(k_2)$ corresponding to the second measurement is excluded.

For the second case, AS particles used for performing the first measurement are recycled in order to participate in the second measurement as well. For this case, which is far less common, the condition $[A_2(t_2), A_1(t_1)] = 0$ can be violated, and consequently, a collapse-induced effect on $p_2(k_2)$ cannot be ruled out. The possibility that the condition $[A_2(t_2), A_1(t_1)] = 0$ is violated raises some concerns regarding the mathematical self-consistency of quantum mechanics [15–17] (note that this is unrelated to compatibility with the principle of causality).

II. OPTICAL INTERFEROMETER

In the proposed experimental setup, a fiber-optic loop mirror (FOLM) [18,19] is employed in order to allow measurements with recycled photons (see Fig. 1). A short optical pulse with a state of polarization (SOP) $|p_i\rangle$ is injected into port a1 of an optical coupler (OC). A ferrimagnetic sphere resonator (FSR) [20,21] is integrated into the fiber loop of the FOLM near port b1 of the OC. Magneto-optic (MO) coupling [22,23] between the optical pulse and the FSR gives rise to both the Faraday-Voigt effect, which accounts for the change in the optical SOP, and the inverse Faraday effect (IFE) [24–32], which accounts for the optically induced change in

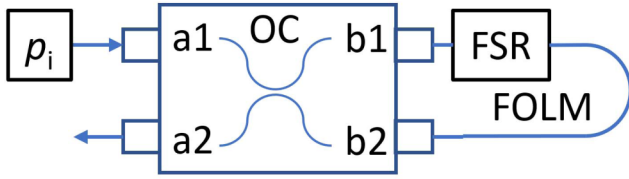


FIG. 1. FOLM interferometer. Light is injected into port a1 of the OC, and detection is performed using a PD connected to port a2. Note that light entering the OC through a port on the left (right) can exit the OC only through ports on the right (left).

the FSR state of magnetization (SOM). The externally injected optical pulse interacts with the FSR at times t_1 and $t_2 > t_1$, and the experimental setup allows the violation of the condition $[A_2(t_2), A_1(t_1)] = 0$, where $A_1(t_1)$ and $A_2(t_2)$ are the corresponding observables. The time difference $t_2 - t_1$ is set by adjusting the length of the fiber loop (labeled FOLM in Fig. 1). The transmitted signal at port a2 of the OC is measured using a photodetector (PD).

The OC is characterized by forward (backward) transmission t (t') and reflection r (r') amplitudes. Incoming amplitudes $\vec{E}_{\text{in}} = (E_{\rightarrow}^{a1} \ E_{\rightarrow}^{a2} \ E_{\leftarrow}^{b1} \ E_{\leftarrow}^{b2})^T$ are related to outgoing amplitudes $\vec{E}_{\text{out}} = (E_{\leftarrow}^{a1} \ E_{\leftarrow}^{a2} \ E_{\rightarrow}^{b1} \ E_{\rightarrow}^{b2})^T$ by $\vec{E}_{\text{out}} = S\vec{E}_{\text{in}}$ (the subscript horizontal arrow indicates the propagation direction, and superscripts indicate the OC port label), where the scattering matrix S is given by (it is assumed that all scattering coefficients are polarization independent)

$$S = \begin{pmatrix} 0 & 0 & t' & r' \\ 0 & 0 & r' & t' \\ t & r & 0 & 0 \\ r & t & 0 & 0 \end{pmatrix}. \quad (1)$$

Unitarity $S^\dagger S = 1$ implies that $|t|^2 + |r|^2 = |t'|^2 + |r'|^2 = 1$ and $\text{Re}(r^*t) = \text{Re}(r'^*t') = 0$. Time reversal symmetry $S^T = S$ implies that $t' = t$ and $r' = r = it|r/t|$.

The transmission (reflection) coefficient t (r) is the amplitude of the subpulse circulating the FOLM in the clockwise (counterclockwise) direction. The MO coupling gives rise to a change in both the optical SOP and the FSR SOM. These states for the clockwise (counterclockwise) direction are labeled $|p_+\rangle_P$ and $|m_+\rangle_M$ ($|p_-\rangle_P$ and $|m_-\rangle_M$), respectively (note that these states, which are allowed to change in time, are assumed to be normalized). The state vector $|\psi_f\rangle$, which represents a final state after the pulse has left the interferometer, can be expressed as

$$|\psi_f\rangle = tr'|a_1 \leftarrow, p_+, m_+\rangle + rt'|a_1 \leftarrow, p_-, m_-\rangle + tt'|a_2 \leftarrow, p_+, m_+\rangle + rr'|a_2 \leftarrow, p_-, m_-\rangle, \quad (2)$$

where $|T, p, m\rangle = |T\rangle_I \otimes |p\rangle_P \otimes |m\rangle_M$ denotes a state with a pulse in interferometer port T, optical polarization p , and FSR magnetization m .

Let $\{|p_{n'}\rangle_P\}$ ($\{|m_{n''}\rangle_M\}$) be an orthonormal basis for the Hilbert space of an optical SOP (FSR SOM). The transmission p_T and reflection p_R probabilities are found by

tracing out

$$p_T = \sum_{n', n''} |\langle \psi_f | (|a_2 \leftarrow\rangle_I \otimes |p_{n'}\rangle_P \otimes |m_{n''}\rangle_M) |^2, \quad (3)$$

$$p_R = \sum_{n', n''} |\langle \psi_f | (|a_1 \leftarrow\rangle_I \otimes |p_{n'}\rangle_P \otimes |m_{n''}\rangle_M) |^2; \quad (4)$$

hence (note that $\sum_{n'} |p_{n'}\rangle_P \langle p_{n'}| = 1_P$ and $\sum_{n''} |m_{n''}\rangle_M \langle m_{n''}| = 1_M$ and recall that $|p_\pm\rangle_P$ and $|m_\pm\rangle_M$ are normalized and that $t' = t$ and $r' = r = it|r/t|$),

$$p_T = (|t|^2 - |r|^2)^2 + 4|tr|^2\eta, \quad (5)$$

$$p_R = 4|tr|^2(1 - \eta), \quad (6)$$

where

$$\eta = \frac{1 - \text{Re}(\chi_P \chi_M)}{2} \quad (7)$$

and $\chi_P = \langle p_+ | p_- \rangle_P$ and $\chi_M = \langle m_+ | m_- \rangle_M$. Note that $p_T + p_R = 1$ (recall that $|t|^2 + |r|^2 = 1$). In the absence of any MO coupling, i.e., when $\chi_P \chi_M = 1$, $\eta = 0$, whereas $\eta = 1/2$ for the opposite extreme case of $\chi_P \chi_M = 0$. For the case of a 3 dB OC (i.e., when $|t|^2 = |r|^2 = 1/2$) this becomes $p_T = \eta$ and $p_R = 1 - \eta$. Thus, in the absence of any MO coupling and for a 3 dB OC the transmission probability p_T vanishes. This unique property, which originates from destructive interference in the FOLM interferometer, allows sensitive measurement of the effect of MO coupling.

The parameter χ_P characterizes the change in SOP induced by the Faraday-Voigt effect, whereas the change in the FSR SOM induced by the IFE [24,33,34] is characterized by the parameter χ_M . Both effects originate from the MO coupling between the optical pulses and the FSR, and the Verdet constant [22,23,29,35] is proportional to induced changes in both SOP and SOM [36] (see also Eq. (2.316) of [37]). Based on Appendix B, which reviews MO coupling, the parameter η is estimated.

Two configurations are considered below. For the first one $\hat{\mathbf{q}} \parallel \mathbf{H}_{\text{dc}}$, whereas $\hat{\mathbf{q}} \perp \mathbf{H}_{\text{dc}}$ for the second configuration, where $\hat{\mathbf{q}}$ is a unit vector parallel to the optical propagation direction and \mathbf{H}_{dc} is the static magnetic field externally applied to the FSR. The angular frequency of the Kittel mode ω_m is related to H_{dc} by $\omega_m = \gamma_e \mu_0 H_{\text{dc}}$, where $\gamma_e/2\pi = 28 \text{ GHz T}^{-1}$ is the gyromagnetic ratio and μ_0 is the free-space permeability (magnetic anisotropy is disregarded). For both cases it is shown below that, on the one hand, the intermediate value of $\text{Re}(\chi_P \chi_M)$ during the time interval $[t_1, t_2]$ can be made significantly smaller than unity, whereas, on the other hand, the final (i.e., after time t_2) value of $\text{Re}(\chi_P \chi_M)$ can be made very close to unity [see Eq. (7)]. Hence, for these cases the transmitted signal at port a2 is strongly affected by the level of unitarity in the time evolution of the system prior to time t_2 .

The change in SOP for the first configuration is dominated by the Faraday effect, whereas the Voigt effect, which is much weaker [see Eqs. (B22), (B23), and (B26) in Appendix B and note that $Q_s \ll 1$], accounts for the change in SOP for the second configuration. In the analysis below, the change in SOP is disregarded for the second configuration (i.e., it is assumed that $\chi_P = 1$).

The IFE gives rise to an effective magnetic field \mathbf{H}_{IFE} , which is parallel to the optical propagation direction $\hat{\mathbf{q}}$, and it has a magnitude proportional to $I_{p+} - I_{p-}$, where I_{p+} (I_{p-}) is the optical energy carried by right-hand (R) (left-hand L) circular SOP [29] [see Eq. (B32) in Appendix B]. With femtosecond optical pulses this optically induced magnetic field \mathbf{H}_{IFE} can be employed for ultrafast manipulation of the SOM [38–40]. For the first configuration (for which $\hat{\mathbf{q}} \parallel \mathbf{H}_{\text{dc}}$), it is expected that the change in the SOM due to the IFE will be relatively small (since $\mathbf{H}_{\text{IFE}} \parallel \mathbf{H}_{\text{dc}}$ and the magnetization is assumed to be nearly parallel to \mathbf{H}_{dc}). In the analysis below, the change in SOM is disregarded for the first configuration (i.e., it is assumed that $\chi_M = 1$). For the second configuration (for which $\hat{\mathbf{q}} \perp \mathbf{H}_{\text{dc}}$), on the other hand, the IFE gives rise to a much larger effect (since \mathbf{H}_{IFE} is nearly perpendicular to the magnetization for this case).

For both configurations the observables A_1 and A_2 represent the photonic spatial location (i.e., the interferometer port T in the state notation $|T, p, m\rangle = |T\rangle_{\text{I}} \otimes |p\rangle_{\text{P}} \otimes |m\rangle_{\text{M}}$). In the proposed setup, photons are recycled; that is, the same photons interact with the FSR at both times t_1 and $t_2 > t_1$ (the times when the partial pulses hit the FSR). Consequently, during the time interval $[t_1, t_2]$ the condition $[A_2(t_2), A_1(t_1)] = 0$ (A11) can be violated. As discussed above, the entangled state created during the time interval $[t_1, t_2]$ is associated with the SOP (SOM) for the first (second) configuration, which is discussed in Sec. III (Sec. IV). This entangled state is made of macroscopic numbers of photons and spins. The level of entanglement is characterized by the parameter η [see Eq. (7)], which can be experimentally determined by measuring the probability p_T [see Eq. (5)]. As will be shown below, for both configurations, the entanglement can be made significant during the time interval $[t_1, t_2]$. Moreover, it can be eliminated at time t_2 , prior to the measurement performed by the PD connected to OC port a2. As will be shown below, the level of disentanglement performed by the second pulse at time t_2 can be tuned. Note that the time interval $[t_1, t_2]$ can be made sufficiently short to make environmental decoherence negligibly small. Hence, the level of nonunitarity in the time evolution of the system can be determined by measuring p_T . The FOLM setup, for which port a2 becomes dark (i.e., $p_T = 0$) in the limit of complete unitarity [provided that $|t|^2 = |r|^2 = 1/2$; see Eq. (5)], allows high detection sensitivity of nonunitarity.

III. THE CASE $\hat{\mathbf{q}} \parallel \mathbf{H}_{\text{dc}}$

The Jones matrices corresponding to clockwise and counterclockwise directions of loop circulation are given by $J_+ = \sigma_z J_S(t_1)$ and $J_- = \sigma_z J_S(t_2) \sigma_z \sigma_z$, respectively, where $J_S(t)$ is the FSR Jones matrix at time t and $\sigma = (\sigma_x, \sigma_y, \sigma_z)$ is the Pauli matrix vector [see Eq. (B21) herein and Eqs. (14.106) and (14.112) of [41] and note that the transmission through the loop gives rise to a mirror reflection of the SOP and that $\sigma_z^2 = 1$]. The term χ_P is thus given by $\chi_P = \langle p_i | J_S^\dagger(t_1) J_S(t_2) | p_i \rangle$.

Let φ_{S1} and φ_{S2} be the rotation angles associated with the unitary transformations $J_S(t_1)$ and $J_S(t_2)$, respectively. For the case $\hat{\mathbf{q}} \parallel \mathbf{H}_{\text{dc}}$, circular birefringence (CB) induced by the Faraday effect is the dominant mechanism giving rise to the change in SOP, and the corresponding Jones matrices $J_S(t_1)$ and $J_S(t_2)$ can be calculated using Eq. (B26) with $\mathbf{k}_B = \mathbf{k}_{\text{CB}}$

[see Eq. (B22)]. As shown in Appendix B, for the Faraday effect, typically, $|\varphi_{S1}| \simeq 0.1$, and $|\varphi_{S2}| \simeq 0.1$ for a magnetically saturated FSR of radius $R_s \simeq 100 \mu\text{m}$. Hence, during the time interval $[t_1, t_2]$, the intermediate value of $\text{Re}(\chi_P)$ is expected to be significantly smaller than unity.

The final (i.e., after time t_2) value of $\text{Re}(\chi_P)$ depends on the rotation angle φ_S associated with the unitary transformations $J_S^\dagger(t_1) J_S(t_2)$. The Jones matrix J_S given by Eq. (B26) in Appendix B is expressed as a function of the FSR SOM. For the case where FSR excitation during the time interval (t_1, t_2) is on the order of a single magnon, one has $|\varphi_S| \simeq (l_e/l_p) \theta_{m0}$, where θ_{m0} is the magnetization rotation angle corresponding to a single magnon excitation. As shown in Appendix B, typically, $l_e/l_p \simeq 10^{-1}$. From the Stoner-Wohlfarth energy E_M given by Eqs. (B27) and (B28) one finds that typically, $\theta_{m0} \simeq 10^{-9}$ (for the transition from the ground state to a single magnon excitation state). Hence, the approximation $\chi_P = 1$ (i.e., $\varphi_S = 0$) can be safely employed in the calculation of η , provided that the number of excited magnons is sufficiently small. The unique configuration of the proposed interferometer allows a finite value of $\text{Re}(\chi_P)$ very close to unity, in spite of the fact that the intermediate value of $\text{Re}(\chi_P)$ can be significantly smaller than unity.

IV. THE CASE $\hat{\mathbf{q}} \perp \mathbf{H}_{\text{dc}}$

For simplicity, consider first the case where the FSR is prepared in its ground state before the optical pulse is applied (i.e., initially, the angle θ_m between the magnetization and the externally applied static magnetic field \mathbf{H}_{dc} vanishes). Let θ_{IFE} be the value of θ_m immediately after the interaction with a pulse carrying a single optical photon. The intermediate value of $\text{Re}(\chi_M)$ during the time interval $[t_1, t_2]$ is expected to be significantly smaller than unity provided that $|\theta_{\text{IFE}}| \gtrsim |\theta_{m0}|$ (recall that θ_{m0} is the magnetization rotation angle corresponding to a single magnon excitation). This condition can be satisfied when angular momentum conversion between photons and magnons is sufficiently efficient [42]. On the other hand, as shown below, the final (i.e., after time t_2) value of $\text{Re}(\chi_M)$ can be made very close to unity. Note that the semiclassical model that is presented in Appendix B allows expressing $|\theta_{m0}|$ as a function of the magnetization tilt angle θ_m and the constant θ_{mz} given by Eq. (B27) [see Eqs. (B28) and (B33)].

The level of entanglement associated with the state $|\psi_f\rangle$ (2) can be characterized by the purity $\varrho_i = \text{Tr} \rho_i^2 = \text{Tr} \rho_M^2$ of the reduced density matrices ρ_i and ρ_M of the optical and FSR subsystems, respectively, which can be extracted from the Schmidt decomposition of $|\psi_i\rangle$ [43]. In the absence of entanglement $\varrho_i = 1$, whereas for a maximized entanglement $\varrho_i = 1/2$. Consider the case of weak excitation, for which the SOM angle θ_m is small. For this case, the Bosonization Holstein-Primakoff transformation [44] can be employed in order to allow the description of the state of the transverse magnetization in terms of a quantum state vector in the Hilbert space of a one-dimensional harmonic oscillator (i.e., a boson). Such a description greatly simplifies the calculation of the purity ϱ_i .

Consider the case where the SOP of the partial pulse hitting the FSR at time t_1 is adjusted to be a circular left-hand

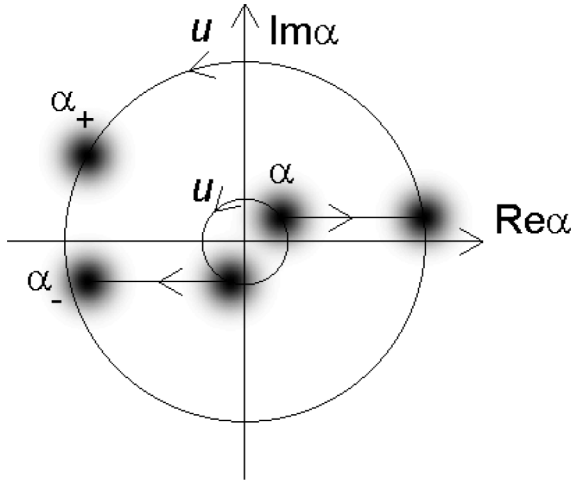


FIG. 2. The coherent states α_+ and α_- . The left to right (right to left) horizontal arrow represents the displacement transformation $D(\alpha_i)$ [$D(-\alpha_i)$]. Note that for the case depicted by this plot, the condition $\cos[\omega_m(t_2 - t_1)/2] = 0$ is not satisfied (and, consequently, $\alpha_+ \neq \alpha_-$).

$|L\rangle$ SOP. For that case the partial pulse hitting the FSR at the later time $t_2 > t_1$ is expected to have a circular right-hand $|R\rangle$ SOP (the loop gives rise to a mirror reflection of the SOP). The precession of the SOM with angular frequency ω_m during the time interval (t_1, t_2) is described by the unitary time evolution operator $u(t_2 - t_1)$, where $u(t) = \exp(-i\omega_m t a_m^\dagger a_m)$ and a_m is a magnon annihilation operator. The change in the SOM induced by the IFE due to the partial pulse hitting the FSR at time t_1 (t_2) is described by a displacement operator $D(\alpha_i)$ [$D(-\alpha_i)$], where the coherent state complex parameter α_i has a length given by $|\alpha_i| = \theta_{\text{IFE}}/\theta_{m0}$. It is assumed that $\omega_m t_p \ll 1$, where t_p is the pulse time duration.

When the initial SOM is assumed to be a coherent state $|\alpha\rangle$ with a complex parameter α , the final SOM corresponding to circulating the FOLM in the clockwise (counterclockwise) direction is a coherent state $|m_+\rangle_M = |\alpha_+\rangle$ ($|m_-\rangle_M = |\alpha_-\rangle$) with complex parameter $\alpha_+ = (\alpha + \alpha_i)e^{-i\omega_m(t_2-t_1)}$ ($\alpha_- = \alpha e^{-i\omega_m(t_2-t_1)} - \alpha_i$) [see Eq. (5.53) of [41] and Fig. 2]. The state vector $|\psi_f\rangle$ can be expressed as $|\psi_f\rangle = v_1|a_1 \leftarrow \right\rangle_I \otimes |m_1\rangle_M + v_2|a_2 \leftarrow \right\rangle_I \otimes |m_2\rangle_M$, where $v_1 = it^2\sqrt{v v_+}$, $|m_1\rangle_M = (|\alpha_+\rangle + |\alpha_-\rangle)/\sqrt{v_+}$, $v_2 = t^2\sqrt{(1-v)^2 + v v_-}$, $|m_2\rangle_M = (|\alpha_+\rangle - v|\alpha_-\rangle)/\sqrt{(1-v)^2 + v v_-}$, and $\mu = \langle\alpha_+|\alpha_-\rangle = \mu' + i\mu''$, with both μ' and μ'' being real, $v = |r/t|^2$, and $v_\pm = 2(1 \pm \mu')$ [see Eq. (2)]. Note that both $|m_1\rangle_M$ and $|m_2\rangle_M$ are normalized. The purity ϱ_i associated with the state $|\psi_f\rangle$ is given by $\varrho_i = 1 - 2|v_1 v_2|^2(1 - |{}_M\langle m_1 | m_2 \rangle_M|^2)$ (see Eq. (8.681) of [41]). For a 3 dB OC, i.e., for $v = |r/t|^2 = 1$, this becomes $\varrho_i = [1 + \exp(-|\alpha_+ - \alpha_-|^2)]/2$ (see Eq. (5.243) of [41]) or (note that ϱ_i is independent of α)

$$\varrho_i = \frac{1 + \exp\left(-4|\alpha_i|^2 \cos^2 \frac{\omega_m(t_2-t_1)}{2}\right)}{2}. \quad (8)$$

The time interval $t_2 - t_1$ can be set by adjusting the length of the fiber loop connecting ports b1 and b2 of the OC.

A delay time of a single FSR period $\omega_m/(2\pi)$ is obtained with a fiber of length L_F , given by $L_F = cn_F^{-1}[\omega_m/(2\pi)]^{-1} = 68 \text{ mm}(n_F/1.47)^{-1}\{[\omega_m/(2\pi)]/(3 \text{ GHz})\}^{-1}$, where n_F is the fiber's effective refractive index. When the ratio $(t_2 - t_1)/(2\pi/\omega_m)$ is much smaller than the FSR quality factor, the effect of magnon damping can be disregarded.

During the time interval (t_1, t_2) the entanglement is nearly maximized provided that $e^{-|\alpha_i|^2} \ll 1$. For a symmetric OC (i.e., for $|r/t| = 1$), a full collapse accruing during this time interval results in a transmission probability $p_T \simeq 1/2$, whereas unitary evolution yields $p_T \simeq 0$. Consider the case where the condition $\cos[\omega_m(t_2 - t_1)/2] = 0$ is satisfied. Note that for this case $u(t_2 - t_1)|\alpha\rangle = |-\alpha\rangle$; hence, the partial pulse hitting the FSR at time t_2 undoes the earlier change that has occurred at time t_1 (recall that the fiber loop gives rise to a mirror transformation $|L\rangle \rightarrow |R\rangle$ in the SOP), and consequently, entanglement is eliminated, and the final state of the system $|\psi_f\rangle$ after time t_2 becomes a product state, i.e., $\text{Re}(\chi_M) = 1$.

In the analysis above the Sagnac effect has been disregarded. In general, this effect, which gives rise to a relative phase shift between the clockwise and counterclockwise partial pulses, can also contribute to the suppression of the destructive interference at the outgoing OC port a2. The Sagnac effect can be eliminated by placing the fiber loop in a plane parallel to earth's rotation axis.

V. SUMMARY

Devices similar to the one discussed here, which are based on ferrimagnetic MO coupling [34,45–48], are currently being developed worldwide [49–51], mainly for the purpose of optically interfacing superconducting quantum circuits. Ultrafast (subpicosecond timescales) laser control of the SOM [38] can be employed for the preparation and manipulation of nonclassical states of a FSR.

The device we proposed here is designed to allow studying the quantum to classical transition associated with the interaction between an optical pulse and a FSR containing $\sim 10^{17}$ spins. The measured transmission probability p_T provides a very sensitive probe for nonunitarity in the system's time evolution. Unitary evolution yields $p_T \simeq 0$, whereas a full collapse occurring during the time interval (t_1, t_2) results in $p_T \simeq 1/2$. The proposed experimental setup allows the generation of an entangled state during the time interval (t_1, t_2) . The level of entanglement after time t_2 can be controlled by adjusting the time duration $t_1 - t_2$ (which can be made much shorter than all timescales characterizing environmental decoherence). Systematic measurements of the transmission probability p_T with varying parameters may provide important insight into the nonunitary nature of a quantum measurement.

ACKNOWLEDGMENTS

This work was supported by the Israeli Science Foundation, the Israeli Ministry of Science, and the Technion Security Research Foundation.

APPENDIX A: SUCCESSIVE MEASUREMENTS

Consider a system whose density operator is denoted by ρ and whose time evolution operator is denoted by u . Two measurements are performed. In the first one, which is performed at time $t_1 \geq t_0$, the observable A_1 is being measured (t_0 is an initial time), whereas in the second one, which is performed at a later time $t_2 \geq t_1$, the observable A_2 is being measured. Let \mathcal{A}_1 be the outcome of the first measurement and \mathcal{A}_2 be the outcome of the second one. Moreover, let $\{a_{n,k}\}_k$ be the set of eigenvalues of the observable A_n , where $n \in \{1, 2\}$.

The unitary time evolution of ρ , corresponding to the case where no measurements are performed (i.e., no collapse), is given by

$$\rho(t) = u(t; t_0)\rho_0 u^\dagger(t; t_0), \quad (\text{A1})$$

where $u(t; t_0)$ is the time evolution operator from time t_0 to time t and $\rho_0 = \rho(t_0)$ is the density operator at initial time t_0 . Each of the two observables A_1 and A_2 can be expressed in terms of its eigenvalues $a_{n,k}$ and in terms of the projection operators $P_{n,k}$ onto the corresponding subspaces as

$$A_n = \sum_k a_{n,k} P_{n,k}, \quad (\text{A2})$$

where the projection operators $P_{n,k}$ are given by

$$P_{n,k} = \prod_{k' \neq k} \frac{A_n - a_{n,k'}}{a_{n,k} - a_{n,k'}}. \quad (\text{A3})$$

The eigenvalues of the Hermitian projection operator $P_{n,k}$ are 0 and 1, and the following holds: $P_{n,k}P_{n,k'} = P_{n,k'}P_{n,k} = P_{n,k}\delta_{k,k'}$. The closure relation is given by

$$\sum_k P_{n,k} = 1. \quad (\text{A4})$$

The probability $p_1(k_1)$ that the measurement at time t_1 of the observable A_1 yields the value a_{1,k_1} , namely, the probability that $\mathcal{A}_1 = a_{1,k_1}$, is given by $p_1(k_1) = \text{Tr}[P_{1,k_1}\rho(t_1)]$. Using Eq. (A1) and the notation $\bar{O} = \text{Tr}(O\rho_0)$, where O is an operator, one finds that the probability $p_1(k_1)$ can be expressed as

$$p_1(k_1) = \overline{P_{1,k_1}(t_1)}, \quad (\text{A5})$$

where $P_{1,k_1}(t_1) = u^\dagger(t_1; t_0)P_{1,k_1}u(t_1; t_0)$ is the Heisenberg representation of the projection operator P_{1,k_1} .

Next, the probability $p_2(k_2)$ that the measurement at time t_2 of the observable A_2 yields the value a_{2,k_2} (i.e., $\mathcal{A}_2 = a_{2,k_2}$) is calculated. According to the collapse postulate, the first measurement at time t_1 disturbs the unitary time evolution given by Eq. (A1) of the density operator ρ . Given that a_{1,k_1} was obtained in the first measurement of A_1 at time t_1 , the density operator $\rho(t_1) = u(t_1; t_0)\rho_0 u^\dagger(t_1; t_0)$ collapses and becomes $\rho_{k_1}(t_1)$, where

$$\rho_{k_1}(t_1) = \frac{P_{1,k_1}\rho(t_1)P_{1,k_1}}{p_1(k_1)}. \quad (\text{A6})$$

By assuming unitary time evolution from time t_1 to time t_2 one finds that the conditional probability $p(k_2|k_1)$ that $\mathcal{A}_2 = a_{2,k_2}$,

given that $\mathcal{A}_1 = a_{1,k_1}$, is given by

$$p(k_2|k_1) = \frac{\overline{P_{1,k_1}(t_1)P_{2,k_2}(t_2)P_{1,k_1}(t_1)}}{p_1(k_1)}, \quad (\text{A7})$$

where $P_{2,k_2}(t_2) = u^\dagger(t_2; t_0)P_{2,k_2}u(t_2; t_0)$. The last result implies that the joint probability $p(k_1, k_2) = p_1(k_1)p(k_2|k_1)$, namely, the probability that $\mathcal{A}_1 = a_{1,k_1}$ and $\mathcal{A}_2 = a_{2,k_2}$, is given by

$$p(k_1, k_2) = \overline{P_{1,k_1}(t_1)P_{2,k_2}(t_2)P_{1,k_1}(t_1)}. \quad (\text{A8})$$

Furthermore, the probability $p_2(k_2)$ that $\mathcal{A}_2 = a_{2,k_2}$ is given by

$$p_2(k_2) = \text{Tr}[P_{2,k_2}u(t_2; t_1)\rho_p u^\dagger(t_2; t_1)], \quad (\text{A9})$$

where the projected density operator ρ_p is given by

$$\rho_p = \sum_{k'_1} P_{1,k'_1}\rho(t_1)P_{1,k'_1}. \quad (\text{A10})$$

Under what conditions is the probability $p_2(k_2)$ for the measurement at time t_2 affected by the collapse due to the earlier measurement at time t_1 ? It is shown below that the collapse has no effect provided that the condition

$$[A_2(t_2), A_1(t_1)] = 0 \quad (\text{A11})$$

is satisfied. This condition implies that for all k_1 and all k_2 the following holds: $[P_{2,k_2}(t_2), P_{1,k_1}(t_1)] = 0$, and therefore, $p(k_1, k_2) = P_{1,k_1}(t_1)P_{2,k_2}(t_2)$ [see Eq. (A8)]. Hence, $p_2(k_2) = \sum_{k'_1} p(k'_1, k_2) = P_{2,k_2}(t_2)$ [see Eq. (A4)]. Thus, for this case the collapse at time t_1 does not affect the measurement at the later time t_2 [compare with Eq. (A5)].

In general, the following holds: $[A_2(t_2), A_1(t_1)] = u^\dagger(t_1; t_0)[u^\dagger(t_2; t_1)A_2u(t_2; t_1), A_1]u(t_1; t_0)$. Hence, the condition $[A_2(t_2), A_1(t_1)] = 0$ is satisfied, provided that there is no interaction between the two different subsystems during the time interval $t \in (t_1, t_2)$ between the two measurements (note that interaction between the subsystems before or after this time interval is not excluded).

APPENDIX B: MAGNETO-OPTICS

In this Appendix the MO Faraday, Voigt, and inverse Faraday effects are briefly reviewed.

1. Macroscopic Maxwell's equations

In the absence of current sources, the macroscopic Maxwell's equations in Fourier space are given by

$$\mathbf{q} \times \mathbf{H}_T(\mathbf{q}, \omega) = -\frac{i\omega}{c} \mathbf{D}(\mathbf{q}, \omega), \quad (\text{B1})$$

$$\mathbf{q} \times \mathbf{E}_T(\mathbf{q}, \omega) = \frac{\omega}{c} \mathbf{B}(\mathbf{q}, \omega), \quad (\text{B2})$$

$$\mathbf{q} \cdot \mathbf{D}_L(\mathbf{q}, \omega) = 4\pi \rho_{\text{ext}}(\mathbf{q}, \omega), \quad (\text{B3})$$

$$\mathbf{q} \cdot \mathbf{B}_L(\mathbf{q}, \omega) = 0, \quad (\text{B4})$$

where \mathbf{H} is the magnetic field, \mathbf{E} is the electric field, \mathbf{B} is the magnetic induction, \mathbf{D} is the electric displacement, ρ_{ext} is the charge density, c is the speed of light, \mathbf{q} is the Fourier wave vector, and ω is the Fourier angular frequency. All vector fields $\mathbf{F} \in \{\mathbf{H}, \mathbf{E}, \mathbf{B}, \mathbf{D}\}$ are decomposed into longitudinal and

transverse parts with respect to the wave vector \mathbf{q} according to $\mathbf{F} = \mathbf{F}_L + \mathbf{F}_T$, where the longitudinal part is given by $\mathbf{F}_L = (\hat{\mathbf{q}} \cdot \mathbf{F})\hat{\mathbf{q}}$, the transverse one is given by $\mathbf{F}_T = (\hat{\mathbf{q}} \times \mathbf{F}) \times \hat{\mathbf{q}}$, and $\hat{\mathbf{q}} = \mathbf{q}/|\mathbf{q}|$ is a unit vector in the direction of \mathbf{q} . For an isotropic and linear medium the following relations hold: $\mathbf{D} = \epsilon_m \mathbf{E}$, where ϵ_m is the permittivity tensor, and $\mathbf{B} = \mu_m \mathbf{H}$, where μ_m is the permeability tensor. In the optical band to a good approximation μ_m is the identity tensor.

By applying $\mathbf{q} \times$ to Eq. (B2) from the left and employing Eq. (B1), one obtains $\mathbf{q} \times (\mathbf{q} \times \mathbf{E}_T) = -\epsilon(\omega/c)^2 \mathbf{E}_T$ [22,52,53], or in matrix form [note that for general vectors \mathbf{u} and \mathbf{v} the following holds: $\mathbf{u} \times (\mathbf{u} \times \mathbf{v}) = (\mathbf{u}\mathbf{u}^T - \mathbf{u} \cdot \mathbf{u})\mathbf{v}$]

$$\left(M_\epsilon + 1 - \frac{n^2}{n_0^2}\right)\mathbf{E}_T = 0, \quad (\text{B5})$$

where the 3×3 matrix M_ϵ is given by

$$M_\epsilon = \frac{\epsilon_m}{n_0^2} + \frac{\mathbf{q}\mathbf{q}^T}{n_0^2 q_0^2} - 1 = \frac{\epsilon_m + n^2 P_{\hat{\mathbf{q}}}}{n_0^2} - 1, \quad (\text{B6})$$

$\mathbf{q} = q\hat{\mathbf{q}}$, $\hat{\mathbf{q}} = (\sin \theta \cos \phi, \sin \theta \sin \phi, \cos \theta)$, $q_0 = \omega/c$, n_0 is the medium refractive index, $n = q/q_0$, and $P_{\hat{\mathbf{u}}} = \hat{\mathbf{u}}\hat{\mathbf{u}}^T$ is a projection matrix associated with a given unit vector $\hat{\mathbf{u}}$ (the 3×3 identity matrix is denoted by 1). Note that $n^2/n_0^2 - 1 \simeq 2(n - n_0)/n_0$, provided that $|n - n_0| \ll n_0$.

For a ferromagnet or a ferrimagnet medium, it is assumed that the elements ϵ_{ij} are functions of the magnetization vector \mathbf{M} . Onsager's time-reversal symmetry relation reads $\epsilon_{ij}(\mathbf{M}) = \epsilon_{ji}(-\mathbf{M})$. Moreover, it is expected that $\epsilon_{ij}(\mathbf{M} = 0) = 0$ for $i \neq j$. The static magnetic field \mathbf{H}_{dc} is assumed to be parallel to the $\hat{\mathbf{z}}$ direction. For the case where \mathbf{M} is parallel to \mathbf{H}_{dc} (i.e., parallel to $\hat{\mathbf{z}}$) the tensor ϵ_m is assumed to have the form [52,53]

$$\frac{\epsilon_m}{n_0^2} = 1 + iQ M_C, \quad (\text{B7})$$

where the matrix M_C is given by

$$M_C = \begin{pmatrix} 0 & -1 & 0 \\ 1 & 0 & 0 \\ 0 & 0 & 0 \end{pmatrix}. \quad (\text{B8})$$

The value of Q corresponding to saturated magnetization is denoted by Q_s . For yttrium iron garnet (YIG) $Q_s \simeq 10^{-4}$ for (free-space) wavelength $\lambda_0 \simeq 1550$ nm in the telecom band [54]. The corresponding polarization beat length l_p is given by $l_p = \lambda_0/(n_0 Q_s) \simeq 7.0$ mm, where $n_0 = 2.19$ is the refractive index of YIG in the telecom band. In this band $l_p/l_A \simeq 0.014$, where $l_A^{-1} = (0.5 \text{ m})^{-1}$ is the YIG absorption coefficient [35,55–57].

To analyze the change in the SOP induced by MO coupling, a rotation transformation is applied to a coordinate system with the z axis parallel to the propagation direction ($\hat{\mathbf{q}}$ in the nonrotated frame). Let M'_ϵ be the transformed matrix that represents the matrix M_ϵ in that coordinate system. For a given unit vector $\hat{\mathbf{u}}$, the rotation matrix $R_{\hat{\mathbf{q}}}$ is defined by the relation $R_{\hat{\mathbf{q}}}\hat{\mathbf{u}} = \hat{\mathbf{z}}$. The unit vector parallel to the magnetization \mathbf{M} is denoted by $\hat{\mathbf{m}} = (\sin \theta_m \cos \phi_m, \sin \theta_m \sin \phi_m, \cos \theta_m)$. The transformed matrix M'_ϵ is given by

$$M'_\epsilon = \frac{R_{\hat{\mathbf{q}}} R_{\hat{\mathbf{m}}}^{-1} \epsilon_m R_{\hat{\mathbf{m}}} R_{\hat{\mathbf{q}}}^{-1} + n^2 P_{\hat{\mathbf{q}}}}{n_0^2} - 1. \quad (\text{B9})$$

Note that Eq. (B9) implies that (note that $R_{\hat{\mathbf{q}}}^{-1} \hat{\mathbf{z}} = \hat{\mathbf{q}}$ and $R_{\hat{\mathbf{q}}}^{-1} = R_{\hat{\mathbf{q}}}^T$)

$$R_{\hat{\mathbf{q}}}^{-1} M'_\epsilon R_{\hat{\mathbf{q}}} = \frac{R_{\hat{\mathbf{m}}}^{-1} \epsilon_m R_{\hat{\mathbf{m}}} + n^2 P_{\hat{\mathbf{q}}}}{n_0^2} - 1 \quad (\text{B10})$$

and

$$R_{\hat{\mathbf{m}}} R_{\hat{\mathbf{q}}}^{-1} M'_\epsilon R_{\hat{\mathbf{q}}} R_{\hat{\mathbf{m}}}^{-1} = \frac{\epsilon_m + n^2 R_{\hat{\mathbf{m}}} P_{\hat{\mathbf{q}}} R_{\hat{\mathbf{m}}}^{-1}}{n_0^2} - 1. \quad (\text{B11})$$

Note also that (see Eq. (6.235) of [41])

$$\frac{R_{\hat{\mathbf{m}}}^{-1} \left(\frac{\epsilon_m}{n_0^2} - 1\right) R_{\hat{\mathbf{m}}}}{iQ_s} = R_{\hat{\mathbf{m}}}^{-1} M_C R_{\hat{\mathbf{m}}} = C_{\hat{\mathbf{m}}}, \quad (\text{B12})$$

where the matrix $C_{\hat{\mathbf{u}}}$, which is defined by

$$C_{\hat{\mathbf{u}}} = \begin{pmatrix} 0 & -\hat{\mathbf{u}} \cdot \hat{\mathbf{z}} & \hat{\mathbf{u}} \cdot \hat{\mathbf{y}} \\ \hat{\mathbf{u}} \cdot \hat{\mathbf{z}} & 0 & -\hat{\mathbf{u}} \cdot \hat{\mathbf{x}} \\ -\hat{\mathbf{u}} \cdot \hat{\mathbf{y}} & \hat{\mathbf{u}} \cdot \hat{\mathbf{x}} & 0 \end{pmatrix}, \quad (\text{B13})$$

is the cross-product matrix corresponding to a given unit vector $\hat{\mathbf{u}}$ and for an arbitrary three-dimensional vector \mathbf{v} the following holds: $\hat{\mathbf{u}} \times \mathbf{v} = C_{\hat{\mathbf{u}}}\mathbf{v}$ (see Eq. (6.243) of [41]). The following holds:

$$C_{\hat{\mathbf{m}}} = M_C + M_\perp + O(\theta_m^2), \quad (\text{B14})$$

where the matrix M_\perp is given by

$$M_\perp = \theta_m \begin{pmatrix} 0 & 0 & \sin \phi_m \\ 0 & 0 & -\cos \phi_m \\ -\sin \phi_m & \cos \phi_m & 0 \end{pmatrix}. \quad (\text{B15})$$

Hence, to first order in θ_m one has [see Eq. (B9) and note that the approximation $(n^2/n_0^2)P_{\hat{\mathbf{z}}} \simeq P_{\hat{\mathbf{z}}}$ is being employed]

$$M'_\epsilon = iQ_s R_{\hat{\mathbf{q}}}(M_C + M_\perp)R_{\hat{\mathbf{q}}}^{-1} + P_{\hat{\mathbf{z}}}, \quad (\text{B16})$$

or [compare with Eq. (B12)]

$$M'_\epsilon = \begin{pmatrix} 0 & -iQ_z & -iQ_y \\ iQ_z & 0 & iQ_x \\ iQ_y & -iQ_x & 1 \end{pmatrix} + iQ_s R_{\hat{\mathbf{q}}} M_\perp R_{\hat{\mathbf{q}}}^{-1}, \quad (\text{B17})$$

where $(Q_x, Q_y, Q_z) = Q_s \hat{\mathbf{q}}$.

An effective 2×2 matrix M_T corresponding to the transverse components of the electric field (spanned by the first two vectors) is evaluated below using Eq. (4.87) of [41]. When terms of order $\theta_m Q_s^2$ are disregarded (it is assumed that $|\theta_m| \ll 1$ and $Q_s \ll 1$), one finds, using the relation

$$\frac{\begin{pmatrix} 1 & 0 & 0 \\ 0 & 1 & 0 \\ 0 & 0 & 0 \end{pmatrix} R_{\hat{\mathbf{q}}} M_\perp R_{\hat{\mathbf{q}}}^{-1} \begin{pmatrix} 1 & 0 & 0 \\ 0 & 1 & 0 \\ 0 & 0 & 0 \end{pmatrix}}{\theta_m \cos(\phi - \phi_m) \sin \theta} = M_C, \quad (\text{B18})$$

that

$$M_T = Q_s \alpha_{CB} \begin{pmatrix} 0 & -i \\ i & 0 \end{pmatrix} + \begin{pmatrix} -Q_y^2 & Q_x Q_y \\ Q_x Q_y & -Q_x^2 \end{pmatrix},$$

where α_{CB} is given by [recall that $\cos(\phi - \phi_m) = \cos \phi \cos \phi_m + \sin \phi \sin \phi_m$]

$$\alpha_{CB} = \frac{Q_z}{Q_s} + \theta_m \cos(\phi - \phi_m) \sin \theta = \hat{\mathbf{q}} \cdot \hat{\mathbf{m}} + O(\theta_m^2), \quad (\text{B19})$$

or

$$M_T = k_0 \sigma_0 + \mathbf{k}_B \cdot \boldsymbol{\sigma}, \quad (\text{B20})$$

where $k_0 = -(\mathcal{Q}_x^2 + \mathcal{Q}_y^2)/2$, σ_0 is the 2×2 identity matrix, the Pauli matrix vector $\boldsymbol{\sigma} = (\sigma_x, \sigma_y, \sigma_z)$ is given by

$$\sigma_x = \begin{pmatrix} 0 & 1 \\ 1 & 0 \end{pmatrix}, \quad \sigma_y = \begin{pmatrix} 0 & -i \\ i & 0 \end{pmatrix}, \quad \sigma_z = \begin{pmatrix} 1 & 0 \\ 0 & -1 \end{pmatrix}, \quad (\text{B21})$$

the birefringence vector \mathbf{k}_B is expressed as $\mathbf{k}_B = \mathbf{k}_{CB} + \mathbf{k}_{LB}$, with (to first order in θ_m)

$$\mathbf{k}_{CB} = Q_s(0, \hat{\mathbf{q}} \cdot \hat{\mathbf{m}}, 0), \quad (\text{B22})$$

and

$$\mathbf{k}_{LB} = Q_s^2 \left(S\left(-\frac{\pi}{4}\right), 0, S\left(\frac{\pi}{4}\right) \right), \quad (\text{B23})$$

where the squeezing transformation $S(\varrho)$ is given by

$$S(\varrho) = \frac{e^{i(\varrho - \frac{\pi}{4})} \mathcal{Q}^2 + e^{-i(\varrho - \frac{\pi}{4})} \mathcal{Q}^{*2}}{4} \quad (\text{B24})$$

and $\mathcal{Q} = (Q_x + iQ_y)/Q_s$.

2. Jones matrices

In general, the transformation between input SOP and output SOP for a given optical element can be described using a Jones matrix J [58]. For the lossless case the matrix J is unitary, and it can be expressed as $J = B(\hat{\mathbf{u}}, \varphi)$, where

$$B(\hat{\mathbf{u}}, \varphi) \doteq \exp\left(-\frac{i\boldsymbol{\sigma} \cdot \hat{\mathbf{u}}\varphi}{2}\right) = \mathbf{1} \cos \frac{\varphi}{2} - i\boldsymbol{\sigma} \cdot \hat{\mathbf{u}} \sin \frac{\varphi}{2}, \quad (\text{B25})$$

$\hat{\mathbf{u}}$ is a unit vector, and φ is a rotation angle. The collinear vertical, horizontal, diagonal, and anti-diagonal SOPs are denoted by $|V\rangle$, $|H\rangle$, $|D\rangle = 2^{-1/2}(|H\rangle + |V\rangle)$, and $|A\rangle = 2^{-1/2}(|H\rangle - |V\rangle)$, respectively, whereas the circular right-hand and left-hand SOPs are denoted by $|R\rangle = 2^{-1/2}(|H\rangle - i|V\rangle)$ and $|L\rangle = 2^{-1/2}(|H\rangle + i|V\rangle)$, respectively. The unit vectors in the Poincaré sphere corresponding to the SOPs $|V\rangle$, $|H\rangle$, $|D\rangle$, $|A\rangle$, $|R\rangle$, and $|L\rangle$ are $\hat{\mathbf{z}}$, $-\hat{\mathbf{z}}$, $\hat{\mathbf{x}}$, $-\hat{\mathbf{x}}$, $-\hat{\mathbf{y}}$, and $\hat{\mathbf{y}}$, respectively.

Consider a FSR with radius R_s and saturated magnetization. When damping is disregarded, the sphere's Jones matrix J_S is given by [see Eqs. (B20) and (B25)]

$$J_S = B\left(\frac{\mathbf{k}_B}{|\mathbf{k}_B|}, \frac{l_e |\mathbf{k}_B|}{l_p Q_s}\right), \quad (\text{B26})$$

where $l_e \simeq 2R_s$ is the effective optical travel length inside the sphere. The first order in Q_s component of $\mathbf{k}_B = \mathbf{k}_{CB} + \mathbf{k}_{LB}$ in the y direction [see Eq. (B22)] gives rise to CB, known as the Faraday effect, whereas the second order in Q_s components in the xz plane give rise to collinear birefringence (LB) known as the Voigt (Cotton-Mouton) effect [see Eq. (B23)]. The eigenvectors corresponding to CB (LB) have circular (collinear) polarization.

3. Stoner-Wohlfarth energy

When anisotropy is disregarded, the Stoner-Wohlfarth energy E_M of the FSR is given by $E_M = -\mu_0 V_s M_s H_{dc} \cos \theta_m$, where μ_0 is the free-space permeability; $V_s = 4\pi R_s^3/3$ is the volume of the sphere with radius R_s ; M_s is the saturation

magnetization ($M_s = 140 \text{ kA/m}$ for YIG at room temperature); H_{dc} is the static magnetic field, which is related to the angular frequency of the Kittel mode ω_m by $H_{dc} = \omega_m/(\mu_0 \gamma_e)$ [59,60]; and θ_m is the angle between the magnetization and static magnetic field vectors [61]. In terms of the angle θ_{mz} , which is given by

$$\theta_{mz} = \frac{2\hbar\gamma_e}{V_s M_s} = \frac{3.2 \times 10^{-17}}{\left(\frac{R_s}{125\mu\text{m}}\right)^3 \frac{M_s}{140\text{kA/m}}}, \quad (\text{B27})$$

the energy E_M can be expressed as

$$E_M = -2\hbar\omega_m \frac{\cos \theta_m}{\theta_{mz}}. \quad (\text{B28})$$

4. IFE effective magnetic field

Consider the case where the second order in Q_s LB induced by the Voigt effect can be disregarded. For this case, for which \mathbf{k}_B becomes parallel to the $\hat{\mathbf{y}}$ direction in the Poincaré space, it is convenient to express the transverse electric field in the basis of circular SOP $\mathbf{E}_T = E_+ \hat{\mathbf{u}}_+ + E_- \hat{\mathbf{u}}_-$, where $\hat{\mathbf{u}}_{\pm} = (e^{\mp i\pi/4}/\sqrt{2}, e^{\pm i\pi/4}/\sqrt{2})^T$ (note that $\sigma_y \hat{\mathbf{u}}_{\pm} = \pm \hat{\mathbf{u}}_{\pm}$). For this case the electric energy density $u_E = (\epsilon_0/2)(\mathbf{E}_T^\dagger \epsilon'_m \mathbf{E}_T)$ can be expressed as [see Eqs. (B9), (B20), and (B22)]

$$u_E = \epsilon_0 \frac{n_+^2 |E_+|^2 + n_-^2 |E_-|^2}{2}, \quad (\text{B29})$$

where $|E_+|^2$ ($|E_-|^2$) is proportional to the intensity of right-hand (R) (left-hand (L)) circular SOP, $n_{\pm} = n_0(1 \pm |\mathbf{k}_{CB}|)^{1/2}$, and $|\mathbf{k}_{CB}| = Q_s |\hat{\mathbf{q}} \cdot \hat{\mathbf{m}}|$. Alternatively, u_E can be expressed as $u_E = u_{E0} + u_{E1}$, where $u_{E0} = (\epsilon_0 n_0^2/2)(|E_+|^2 + |E_-|^2)$ and $u_{E1} = (\epsilon_0 n_0^2 |\mathbf{k}_{CB}|/2)(|E_+|^2 - |E_-|^2)$. When the energy density is uniformly distributed inside the FSR, the energy $U_T = V_s u_{E1}$ is given by $U_T = \hbar\omega_e |\mathbf{k}_{CB}| = \hbar\omega_e Q_s (\hat{\mathbf{q}} \cdot \hat{\mathbf{m}})$ [see Eq. (B22)], where

$$\omega_e = \frac{\epsilon_0 n_0^2 V_s (|E_+|^2 - |E_-|^2)}{2\hbar}, \quad (\text{B30})$$

or

$$U_T = \frac{\mu_0}{2} \mathbf{H}_{\text{IFE}} \cdot \mathbf{M}, \quad (\text{B31})$$

where the IFE effective magnetic field \mathbf{H}_{IFE} is given by

$$\mathbf{H}_{\text{IFE}} = \frac{2\hbar\omega_e Q_s}{\mu_0 V_s M_s} \hat{\mathbf{q}} = \frac{\omega_e Q_s}{\mu_0 \gamma_e} \theta_{mz} \hat{\mathbf{q}}. \quad (\text{B32})$$

Note that the above result (B32), which is based on a semi-classical model [62,63], was found to underestimate the experimentally measured H_{IFE} by several orders of magnitude [31,64]. A photon-magnon scattering model is employed in [65–67] to evaluate \mathbf{H}_{IFE} . For a single photon excitation $\omega_e = 2\pi c/\lambda$, where λ is the optical wavelength, the corresponding rotation angle of the magnetization, which is denoted by θ_{IFE} , is given by [see Eq. (B32)]

$$\theta_{\text{IFE}} = \mu_0 \gamma_e H_{\text{IFE}} \frac{2n_0 R_s}{c}; \quad (\text{B33})$$

hence, $\theta_{\text{IFE}} = 4\pi n_0 Q_s R_s \theta_{mz}/\lambda$, or $\theta_{\text{IFE}} = 0.18(n_0/2.19)(Q_s/10^{-4})(R_s/100\mu\text{m})(\lambda/1550 \text{ nm})^{-1} \theta_{mz}$.

- [1] L. M. Johansen and P. A. Mello, Quantum mechanics of successive measurements with arbitrary meter coupling, *Phys. Lett. A* **372**, 5760 (2008).
- [2] E. Schrodinger, Die gegenwartige situation in der quantenmechanik, *Naturwissenschaften* **23**, 807 (1935).
- [3] A. J. Leggett, Testing the limits of quantum mechanics: Motivation, state of play, prospects, *J. Phys.: Condens. Matter* **14**, R415 (2002).
- [4] Y. Aharonov and D. Z. Albert, Can we make sense out of the measurement process in relativistic quantum mechanics?, *Phys. Rev. D* **24**, 359 (1981).
- [5] N. D. Mermin, Is the moon there when nobody looks? Reality and the quantum theory, *Phys. Today* **38**(4), 38 (1985).
- [6] J. E. Mooij, Quantum mechanics: No moon there, *Nat. Phys.* **6**, 401 (2010).
- [7] J. Bell, Against ‘measurement,’ *Phys. World* **3**, 33 (1990).
- [8] W. H. Zurek, Pointer basis of quantum apparatus: Into what mixture does the wave packet collapse?, *Phys. Rev. D* **24**, 1516 (1981).
- [9] J. von Neumann, *Mathematical Foundations of Quantum Mechanics* (Princeton University Press, Princeton, NJ, 1983).
- [10] Y. Aharonov and L. Vaidman, Properties of a quantum system during the time interval between two measurements, *Phys. Rev. A* **41**, 11 (1990).
- [11] A. Peres, *Quantum Theory: Concepts and Methods* (Kluwer Academic, Dordrecht, 1993).
- [12] V. B. Braginsky and F. Ya. Khalili, *Quantum Measurement* (Cambridge University Press, Cambridge, 1992).
- [13] R. Ruskov, A. N. Korotkov, and A. Mizel, Signatures of Quantum Behavior in Single-Qubit Weak Measurements, *Phys. Rev. Lett.* **96**, 200404 (2006).
- [14] A. J. Leggett and A. Garg, Quantum Mechanics versus Macroscopic Realism: Is the Flux There When Nobody Looks?, *Phys. Rev. Lett.* **54**, 857 (1985).
- [15] R. Penrose, Uncertainty in quantum mechanics: Faith or fantasy?, *Philos. Trans. R. Soc. A* **369**, 4864 (2011).
- [16] A. J. Leggett, Experimental approaches to the quantum measurement paradox, *Found. Phys.* **18**, 939 (1988).
- [17] A. J. Leggett, Realism and the physical world, *Rep. Prog. Phys.* **71**, 022001 (2008).
- [18] D. B. Mortimore, Fiber loop reflectors, *J. Lightwave Technol.* **6**, 1217 (1988).
- [19] B. Ibarra-Escamilla, E. A. Kuzin, O. Pottiez, J. W. Haus, F. Gutierrez-Zainos, R. Grajales-Coutiño, and P. Zaca-Moran, Fiber optical loop mirror with a symmetrical coupler and a quarter-wave retarder plate in the loop, *Opt. Commun.* **242**, 191 (2004).
- [20] C. Kittel *et al.*, *Introduction to Solid State Physics*, 8th Edition (Wiley, New York, 1976).
- [21] C.-Z. Chai, H.-Q. Zhao, H. X. Tang, G.-C. Guo, C.-L. Zou, and C.-H. Dong, Non-reciprocity in high-q ferromagnetic microspheres via photonic spin-orbit coupling, *Laser Photonics Rev.* **14**, 1900252 (2020).
- [22] Ml. Freiser, A survey of magneto-optic effects, *IEEE Trans. Magn.* **4**, 152 (1968).
- [23] P. S. Pershan, Magneto-optical effects, *J. Appl. Phys.* **38**, 1482 (1967).
- [24] C. Braggio, G. Carugno, M. Guarise, A. Ortolan, and G. Ruoso, Optical Manipulation of a Magnon-Photon Hybrid System, *Phys. Rev. Lett.* **118**, 107205 (2017).
- [25] M. Colautti, Optical manipulation of magnetization of a ferromagnet YIG sphere, Università degli studi di Padova, 2016, <http://tesi.cab.unipd.it/53538/>.
- [26] A. Kirilyuk, A. V. Kimel, and T. Rasing, Ultrafast optical manipulation of magnetic order, *Rev. Mod. Phys.* **82**, 2731 (2010).
- [27] A. Kirilyuk, A. V. Kimel, and T. Rasing, Laser-induced magnetization dynamics and reversal in ferrimagnetic alloys, *Rep. Prog. Phys.* **76**, 026501 (2013).
- [28] A. V. Kimel, A. Kirilyuk, P. A. Usachev, R. V. Pisarev, A. M. Balbashov, and Th. Rasing, Ultrafast non-thermal control of magnetization by instantaneous photomagnetic pulses, *Nature (London)* **435**, 655 (2005).
- [29] J. P. Van der Ziel, P. S. Pershan, and L. D. Malmstrom, Optically-Induced Magnetization Resulting from the Inverse Faraday Effect, *Phys. Rev. Lett.* **15**, 190 (1965).
- [30] P. S. Pershan, J. P. Van der Ziel, and L. D. Malmstrom, Theoretical discussion of the inverse faraday effect, raman scattering, and related phenomena, *Phys. Rev.* **143**, 574 (1966).
- [31] F. Hansteen, A. Kimel, A. Kirilyuk, and T. Rasing, Nonthermal ultrafast optical control of the magnetization in garnet films, *Phys. Rev. B* **73**, 014421 (2006).
- [32] A. Kirilyuk, A. Kimel, F. Hansteen, T. Rasing, and R. V. Pisarev, Ultrafast all-optical control of the magnetization in magnetic dielectrics, *Low Temp. Phys.* **32**, 748 (2006).
- [33] N. Crescini, C. Braggio, G. Carugno, R. Di Vora, A. Ortolan, and G. Ruoso, Magnon-driven dynamics of a hybrid system excited with ultrafast optical pulses, *Commun. Phys.* **3**, 164 (2020).
- [34] R. Hisatomi, A. Osada, Y. Tabuchi, T. Ishikawa, A. Noguchi, R. Yamazaki, K. Usami, and Y. Nakamura, Bidirectional conversion between microwave and light via ferromagnetic magnons, *Phys. Rev. B* **93**, 174427 (2016).
- [35] S. Donati, V. Annovazzi-Lodi, and T. Tambosso, Magneto-optical fibre sensors for electrical industry: Analysis of performances, *IEE Proc.-J: Optoelectron.* **135**, 372 (1988).
- [36] M. Battiato, G. Barbalinardo, and P. M. Oppeneer, Quantum theory of the inverse Faraday effect, *Phys. Rev. B* **89**, 014413 (2014).
- [37] E. Buks, Wave phenomena, <http://buchs.net.technion.ac.il/teaching/>.
- [38] A. V. Kimel, A. Kirilyuk, and T. Rasing, Femtosecond optomagnetism: Ultrafast laser manipulation of magnetic materials, *Laser Photonics Rev.* **1**, 275 (2007).
- [39] D. M. Juraschek, D. S. Wang, and P. Narang, Sum-frequency excitation of coherent magnons, *Phys. Rev. B* **103**, 094407 (2021).
- [40] D. M. Juraschek, P. Narang, and N. A. Spaldin, Phonomagnetic analogs to opto-magnetic effects, *Phys. Rev. Research* **2**, 043035 (2020).
- [41] E. Buks, Quantum mechanics, <http://buchs.net.technion.ac.il/teaching/>.
- [42] S. R. Woodford, Conservation of angular momentum and the inverse Faraday effect, *Phys. Rev. B* **79**, 212412 (2009).
- [43] A. Ekert and P. L. Knight, Entangled quantum systems and the schmidt decomposition, *Am. J. Phys.* **63**, 415 (1995).
- [44] T. Holstein and Hl. Primakoff, Field dependence of the intrinsic domain magnetization of a ferromagnet, *Phys. Rev.* **58**, 1098 (1940).

- [45] E. Almpanis, Dielectric magnetic microparticles as photomagnonic cavities: Enhancing the modulation of near-infrared light by spin waves, *Phys. Rev. B* **97**, 184406 (2018).
- [46] R. Hisatomi, A. Noguchi, R. Yamazaki, Y. Nakata, A. Gloppe, Y. Nakamura, and K. Usami, Helicity-Changing Brillouin Light Scattering by Magnons in a Ferromagnetic Crystal, *Phys. Rev. Lett.* **123**, 207401 (2019).
- [47] P. A. Pantazopoulos, N. Stefanou, E. Almpanis, and N. Papanikolaou, Photomagnonic nanocavities for strong light–spin-wave interaction, *Phys. Rev. B* **96**, 104425 (2017).
- [48] S. Sharma, Y. M. Blanter, and G. E. W. Bauer, Light scattering by magnons in whispering gallery mode cavities, *Phys. Rev. B* **96**, 094412 (2017).
- [49] D. Lachance-Quirion, Y. Tabuchi, A. Gloppe, K. Usami, and Y. Nakamura, Hybrid quantum systems based on magnonics, *Appl. Phys. Express* **12**, 070101 (2019).
- [50] S. P. Wolski, D. Lachance-Quirion, Y. Tabuchi, S. Kono, A. Noguchi, K. Usami, and Y. Nakamura, Dissipation-Based Quantum Sensing of Magnons with a Superconducting Qubit, *Phys. Rev. Lett.* **125**, 117701 (2020).
- [51] N. Zhu, X. Zhang, X. Han, C.-L. Zou, C. Zhong, C.-H. Wang, L. Jiang, and H. X. Tang, Waveguide cavity optomagnonics for broadband multimode microwave-to-optics conversion, [arXiv:2005.06429](https://arxiv.org/abs/2005.06429).
- [52] A. D. Boardman and M. Xie, Magneto-optics: A critical review, in *Introduction to Complex Mediums for Optics and Electromagnetics*, Vol. 123 (2003), p. 197.
- [53] A. D. Boardman and L. Velasco, Gyroelectric cubic-quintic dissipative solitons, *IEEE J. Sel. Top. Quantum Electron.* **12**, 388 (2006).
- [54] D. L. Wood and J. P. Remeika, Effect of impurities on the optical properties of yttrium iron garnet, *J. Appl. Phys.* **38**, 1038 (1967).
- [55] Y. Zhang, C. T. Wang, X. Liang, B. Peng, H. P. Lu, P. H. Zhou, L. Zhang, J. X. Xie, L. J. Deng, M. Zahradnik, L. Beran, M. Kucera, M. Veis, C. A. Ross, and L. Bi, Enhanced magneto-optical effect in $Y_{1.5}Ce_{1.5}Fe_5O_{12}$ thin films deposited on silicon by pulsed laser deposition, *J. Alloys Compd.* **703**, 591 (2017).
- [56] M. C. Onbasli, L. Beran, M. Zahradnik, M. Kučera, R. Antoš, J. Mistrík, G. F. Dionne, M. Veis, and C. A. Ross, Optical and magneto-optical behavior of cerium yttrium iron garnet thin films at wavelengths of 200–1770 nm, *Sci. Rep.* **6**, 23640 (2016).
- [57] Ch. Jooss, J. Albrecht, H. Kuhn, S. Leonhardt, and H. Kronmüller, Magneto-optical studies of current distributions in high- T_c superconductors, *Rep. Prog. Phys.* **65**, 651 (2002).
- [58] R. J. Potton, Reciprocity in optics, *Rep. Prog. Phys.* **67**, 717 (2004).
- [59] P. C. Fletcher and R. O. Bell, Ferrimagnetic resonance modes in spheres, *J. Appl. Phys.* **30**, 687 (1959).
- [60] S. Sharma, Cavity optomagnonics: Manipulating magnetism by light, Ph.D. thesis, Delft University of Technology, 2019.
- [61] D. D. Stancil and A. Prabhakar, *Spin Waves* (Springer, 2009).
- [62] S. V. Kusminskiy, Cavity optomagnonics, in *Optomagnonic Structures: Novel Architectures for Simultaneous Control of Light and Spin Waves* (World Scientific, Singapore, 2021), pp. 299–353.
- [63] N. Zhu, X. Zhang, X. Han, C.-L. Zou, and H. X. Tang, Inverse Faraday effect in an optomagnonic waveguide, [arXiv:2012.11119](https://arxiv.org/abs/2012.11119).
- [64] R. V. Mikhaylovskiy, E. Hendry, and V. V. Kruglyak, Ultrafast inverse Faraday effect in a paramagnetic terbium gallium garnet crystal, *Phys. Rev. B* **86**, 100405 (2012).
- [65] S. M. Rezende, *Fundamentals of Magnonics*, Lecture Notes in Physics, Vol. 969 (Springer, 2020), 1st ed.
- [66] P. A. Fleury and R. Loudon, Scattering of light by one- and two-magnon excitations, *Phys. Rev.* **166**, 514 (1968).
- [67] J. R. Sandercock and W. Wettling, Light scattering from thermal acoustic magnons in yttrium iron garnet, *Solid State Commun.* **13**, 1729 (1973).